CHINESE OPTICS LETTERS

Vol. 20, No. 5 | May 2022

Efficiency-enhanced reflective nanosieve holograms

Samia Osman Hamid Mohammed[1], Dong Zhao (赵 东)[1], Syed Yasir Azeem[1], Xiaoming Goh[2], Shawn J. Tan[2], Jinghua Teng[2**], and Kun Huang (黄 坤)[1*]

[1] Department of Optics and Optical Engineering, University of Science and Technology of China, Hefei 230026, China

[2] Institute of Materials Research and Engineering, Agency for Science, Technology and Research (A*STAR), Singapore 138634, Singapore

*Corresponding author: huangk17@ustc.edu.cn

**Corresponding author: jh-teng@imre.a-star.edu.sg

Received January 14, 2022 | Accepted March 1, 2022 | Posted Online March 24, 2022

Photon nanosieves, as amplitude-type metasurfaces, have been demonstrated usually in a transmission mode for optical super-focusing, display, and holography, but the sieves with subwavelength size constrain optical transmission, thus leading to low efficiency. Here, we report reflective photon nanosieves that consist of metallic meta-mirrors sitting on a transparent quartz substrate. Upon illumination, these meta-mirrors offer the reflectance of ∼50%, which is higher than the transmission of visible light through diameter-identical nanoholes. Benefiting from this configuration, a meta-mirror-based reflective hologram has been demonstrated with good consistence between theoretical and experimental results over the broadband spectrum from 500 nm to 650 nm, meanwhile exhibiting total efficiency of ∼7%. Additionally, if an additional high-reflectance layer is employed below these meta-mirrors, the efficiency can be enhanced further for optical anti-counterfeiting.

Keywords: metasurfaces; nanosieves; holograms; reflective mirrors.

DOI: 10.3788/COL202220.053602

1. Introduction

Photon sieves composed of etched holes on an opaque film have been proposed firstly, to the best of our knowledge, to reduce the focal spot size and alleviate high diffraction orders in soft X-ray and the optical spectrum[1]. With the rapid development of nano-fabrication technology, photon sieves have been demonstrated at nanoscale and worked as binary-amplitude metasurfaces for optical focusing[2,3]. The photon nanosieves have the advantages of polarization independence and more degrees of freedom in design than the concentric rings in zone plates[4], which therefore enable more complex manipulation of light, such as hologram[2,5], by arranging the locations of holes in a customized way. Due to the subwavelength feature of nanosieves, their related holograms usually support broadband operation[6]. In addition, the non-resonating mechanism of amplitude modulation makes the nanosieve hologram have a wider spectrum than other metasurface devices with resonating nano-structures[7]. The nanosieve hologram also enables a large field of view for holographic display when combined with tunable phase realized by a spatial light modulator[8]. Beyond the circular shape, rectangle nanosieves have also been proposed to control the geometric phase of a circularly polarized light by rotating the orientations of the rectangular nanosieves[9,10], thus enabling full-color holography[11] and the generation of optical vortices[10,12–14] in various electromagnetic spectra such as X-ray and vacuum ultraviolet wavelengths[7,15,16].

All of these reported nanosieves operate in a transmission mode, where optical transmission of light through the nanosieves is low because of the weak coupling between the propagating light and the waveguide modes supported within the nanoholes[2,17]. Persistent efforts have been made to solve this efficiency issue. For example, a 15-layer MoS_2 film with a thickness of 10 nm can enhance the coupling for higher transmission, meanwhile blocking the undesired background with strong exciton absorption[18]. The resulting hologram has a record-high efficiency of ∼22%, where the contribution from the background light is also involved. Dielectric nanobricks located at only specially chosen positions, as an extension of classic photon nanosieves, are used to sieve the circularly polarized light with an additional geometric phase for realizing a wavelength- and polarization-sensitive hologram[19]. Although their demonstrated efficiency for one single channel is only 2% at the wavelength of 670 nm due to small bandgap of the employed silicon, it indeed generalizes the concept of photon sieves, hereby suggesting new approaches for improving the efficiency of photon nanosieves.

Here, we generalize the concept of the photon nanosieve by proposing well-designed and location-optimized meta-mirrors that could sieve the reflected photons for holography. These

aluminum meta-mirrors are located on a transparent quartz substrate, working as an analogue of transmissive photon nanosieves. Although the reflective photon sieves (with their dimensions larger than the operating wavelengths) have been proposed at the extreme ultraviolet (EUV) wavelengths for optical focusing[20], our reported nanosieves are subwavelength at the interested visible spectrum and exhibit stronger electromagnetic interaction between light and nanosieves than the EUV case. More importantly, our demonstration is focused on the meta-mirror hologram that has an experimental efficiency of ~7% over a broad visible spectrum, exhibiting an enhancement factor of ~3.5 compared with the previous transmissive nanosieves[2,6].

2. Design Principle

The working principle of the proposed reflective nanosieves is sketched in Fig. 1(a), where the meta-mirrors with subwavelength diameters are used to reflect the incident light. By controlling the locations of these meta-mirrors, one customizes the expected optical field at the target plane. Under such a configuration, the efficiency of the meta-mirror is determined by its geometry, such as the diameter, height, and period, as well as the material constructing the meta-mirror. Compared with other metals such as silver and gold, aluminum is employed here due to the lower cost and less absorption of visible and ultraviolet light. For these aluminum meta-mirrors, their periods along the x and y directions are chosen to be 250 nm, which is almost below half of the entire visible wavelength. In addition, the heights of these aluminum meta-mirrors are optimized to be 100 nm, which is a good balance between optical efficiency and fabrication issues. For example, at the chosen height, the meta-mirrors with an optimized diameter of 200 nm could yield optical reflectance of ~50% at the interested wavelengths from 450 nm to 650 nm [Fig. 1(b)], which cover the preferred red, green, and blue colors in optical display. If the thicker aluminum is used, its high-reflectance spectrum might shift out of this region due to the electromagnetic resonances. Similarly, the thinner aluminum cannot reflect light efficiently. Therefore, the reported meta-mirrors have a height of 100 nm and a diameter of 200 nm in a subwavelength period of 250 nm. Note that the photons reflected by the meta-mirrors are sieved for manipulation of light, while the transmitted photons through the transparent substrate are not used in this work.

We compare the broadband reflectance for these meta-mirrors with the transmission for the classic photon nanosieves. For a fair comparison, the heights, diameters, and periods are equal for both cases of meta-mirrors and nanosieves. The simulated results implemented by using the finite-difference time-domain (FDTD) method are presented in Figs. 1(b) and 1(c), which exhibit higher reflectance for the meta-mirrors than the transmission for the classic nanosieves at the different diameters over a broadband spectrum. It reveals an enhancement factor of ~8 at the 650 nm wavelength, hereby verifying the potential performance enhancement of the proposed meta-mirrors in theory. Note that, although the classic photon nanosieves made in the thinner film can offer high transmission[18], its cost is the increasing undesired background. Therefore, we compare the performance of both cases at the thickness of 100 nm, which could exclude the background efficiently.

Based on this meta-mirror platform, we design a hologram to verify the efficiency, as sketched in Fig. 2(a). In our simulation, the hologram has the pixel number of 800 × 800, where each pixel has a pitch of 250 nm × 250 nm, thus leaving the total size of 200 μm × 200 μm. The distance between the meta-mirror and the target plane is 1 mm, which is large enough for experimental recording of the holographic image. To optimize such a hologram, we employ our previous modified genetic algorithm with only the mutation operation[2], where the optical field diffracting from each meta-mirror can be approximated by using the field from a point source[6,21]. During the optimization, the value of one for one pixel indicates that a meta-mirror exists at

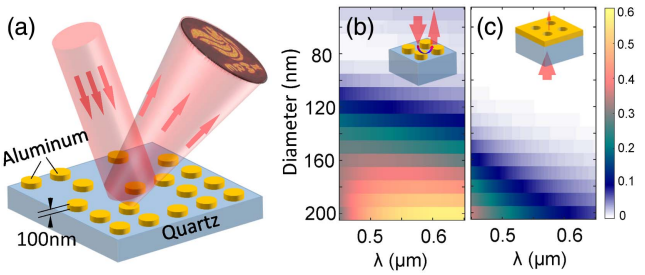

Fig. 1. (a) Sketch of reflective nanosieves composed of aluminum meta-mirrors that could sieve reflective photons for holography. (b) Reflectance of visible light from the 100-nm-height meta-mirrors with different diameters from 50 nm to 200 nm. (c) Transmission of light through the classic nanosieves. To be consistent, the thicknesses of meta-mirrors and nanoholes are 100 nm, and their periods are also kept with the same value of 250 nm. Both nano-mirrors and nanoholes have the same diameters from 50 nm to 200 nm.

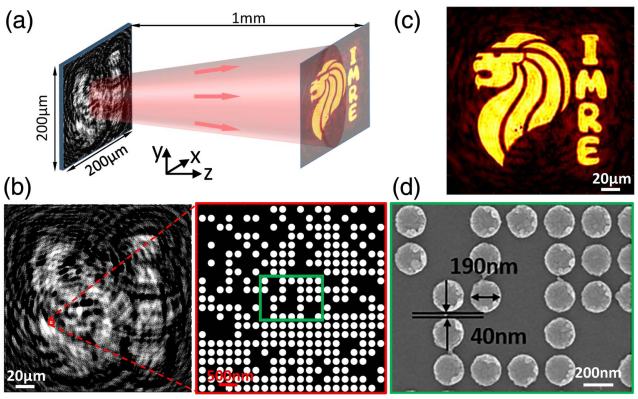

Fig. 2. (a) Sketch of meta-mirror-based hologram. The total size of the hologram is 200 μm × 200 μm. (b) Designed meta-mirrors for the hologram. The white region stands for the meta-mirrors. The right panel shows the zoomed-in pattern, which clearly gives the details of meta-mirrors. (c) Simulated intensity profile at the target plane of z_0 = 1 mm at the wavelength of λ_0 = 532 nm. (d) Scanning-electron-microscopy (SEM) image of the fabricated meta-mirrors. It displays the region encircled within the green rectangle in (b).

this pixel, while the value of zero stands for the case of no meta-mirror. Thus, we can address every meta-mirror and superpose their electric fields coherently, hereby achieving the total field at the target plane. Considering that all these meta-mirrors have the same geometry, the total field depends on only the locations of meta-mirrors. Thus, the aim of this modified genetic algorithm is to optimize the positions of meta-mirrors so that the resulting field is convergent to the ideal pattern, i.e., a lion with four letters "IMRE". Quantitatively, the root-mean-square error (RMSE) between the simulated intensity and the ideal pattern is employed as a cost function to optimize the hologram. The smaller RMSE means the better hologram design. The optimization is a process of minimizing the RMSE. In one iteration, we need the ergodic addressing of 800×800 positions in a random way (realized by using a self-made program). To finalize the design, 10 iterations are used during our optimization. Figures 2(b) and 2(c) show the designed meta-mirrors with nearly random distribution and the simulated intensity profile, respectively. Note that, because only the mutation operation exists in the modified genetic algorithm, the number of the population is employed to be one for accelerating the optimization, implying that the local optimal solution is obtained in our case. However, as observed from the simulated intensity profiles in Fig. 2(c), such a local optimal solution satisfies the requirement for optical holographic images.

3. Experimental Results

To verify it experimentally, we fabricate the designed meta-mirrors by using the e-beam lithography (EBL) technique. A bare quartz substrate is coated with positive-tone resist polymethyl methacrylate (PMMA) at 3000 r/min to a thickness of 180 nm. The designed meta-mirrors patterns are created in PMMA by using EBL (Elionix ELS-7000) at an accelerating voltage of 100 kV and a beam current of 500 pA. Then, the pattern is developed with a 1:3 methyl isobutyl ketone/isopropyl acetone (MIBK/IPA) liquid, removing the exposed regions where the meta-mirrors should be located. After a dry blowing by N_2, the developed sample is deposited with a 100-nm-thick aluminum at a rate of 2 Å/s (1 Å = 0.1 nm) by using an electron-beam evaporator (Explorer Coating System, Denton Vacuum Inc.). Finally, the expected meta-mirrors shown in Fig. 2(d) are formed by lift-off process. The achieved meta-mirrors have the diameters of 190 nm, which approaches the tightly designed value of 200 nm. The inhomogeneity at the surface of aluminum meta-mirrors is caused by the inevitable grain[22] during the deposition process.

The performance of the aluminum meta-mirror photon nanosieves is characterized by using the experimental set-up shown in Fig. 3(a). A supercontinuum laser (SuperK FIANIUM) is employed as the illuminating source with the tunable wavelength that is controlled by an acousto-optic modulator. A spherical lens and an objective lens 1 (20×) are used to create a convergent wave that works as a point source for illuminating the sample. Note that the distance (labelled as d) between the

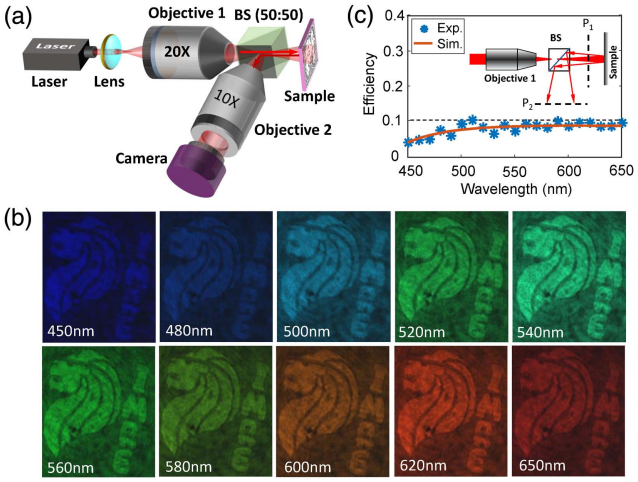

Fig. 3. (a) Experimental setup for the meta-mirror hologram characterization. BS: beam splitter. (b) Measured intensity profiles (raw data) at the exemplified wavelengths. (c) Simulated (curve) and experimental (asterisks) efficiency at the interested wavelengths.

point source and sample is slightly larger than $z_0 = 1$ mm, so that the holographic image is projected at the position $z_t = z_0 \cdot d/(d - z_0)$, which is called the lensing effect of the Fresnel hologram[6]. Meanwhile, the holographic image is magnified with a factor of $M = z_t/d$, facilitating its experimental capture. Considering the reflective operation mode, we put a 50:50 beam splitter between the sample and objective 1 so that the reflected light can be collected by objective lens 2 (10×) and then imaged onto a color camera (Thorlabs CS505CU).

Figure 3(b) shows the measured intensity profiles at the exemplified wavelengths from 450 nm to 650 nm. These holographic images cover blue, green, yellow, and red colors, which makes this technique suitable for optical static display. It therefore confirms the validity of this hologram at a broadband spectrum of 200 nm width. Importantly, the imaging plane shifts at the different wavelength with a dispersion relationship of $z\lambda = z_0\lambda_0$, where z is the distance between the imaging plane at the wavelength λ and the meta-mirror hologram[6]. Due to the Fresnel imaging location of the demonstrated hologram[23], these reconstructed images have the same size, which is similar to the case of classic photon nanosieves. In addition, no aberration or distortion is observed at the recorded images, implying good quality of the holographic reconstruction.

To characterize the efficiency experimentally, we decrease the size of the incident beam so that light is only shining within the area (i.e., 200 μm × 200 μm) of the meta-mirror hologram, thus excluding optical reflectance of quartz outside the meta-mirror region. The incident power is recorded by a power meter (Thorlabs model) at the position P_1 [see the insert in Fig. 3(c)] and taken as I_{in}. Similarly, the power of the holographic image is measured by the same power meter at the position P_2 and labelled as I_{out}. Note that the filling factor [defined by the ratio of the meta-mirror number in the hologram to the total number (i.e., 800×800) of all the pixels] of our designed meta-mirror is only 20%. It means that 80% of the meta-mirror hologram

is the quartz substrate, which leads to the undesired optical reflectance. Thus, the recorded power $I_{out} = 20\% \cdot I_{meta} + 80\% \cdot I_{sub}$, where I_{meta} and I_{sub} are assumed to be the reflected power from the meta-mirrors (100% filled in the region of 200 μm × 200 μm) and the substrate (200 μm × 200 μm), respectively. The signal light is extracted as $I_{signal} = I_{out} \cdot \gamma$, where $\gamma = 1/(1 + 4I_{sub}/I_{meta})$. The ratio I_{sub}/I_{meta} can be obtained by using the ratio of optical reflectance from the periodic meta-mirror and the bare substrate. Thus, the total efficiency of the meta-mirror hologram is $\eta = 2 \cdot I_{signal}/I_{in} = 2\gamma \cdot I_{out}/I_{in}$, where the factor of 2 is multiplied because the 50:50 beam splitter only guides 50% of the signal light to the power meter. Figure 3(c) shows the experimental efficiency η, which agrees very well with the simulated efficiency that is evaluated by $\eta = RF \cdot \mathrm{DE}$, where R is the reflectance of the meta-mirrors, the filling factor $F = 20\%$, and the diffraction efficiency (defined by the ratio of the power of holographic image to the reflected energy purely from the meta-mirror) DE = 75% over the entire spectrum of interest. As observed in Fig. 3(c), the efficiency of ∼7% is obtained at the wavelengths from 500 nm to 650 nm. The slight fluctuation in the measured efficiency originates mainly from the environmental light and the unstable coupling between the supercontinuum laser and the output fiber. Compared with the efficiency of 2% for their counterpart classical photon nanosieves[2,6], the proposed reflective nanosieves have an enhanced efficiency with a factor of 3.5.

4. Discussions

As a comparison among those efficiency-enhanced nanosieves, all of them are aimed at improving the transmission or reflectance of the sieved photons[18,19]. But, as binary-amplitude devices, their theoretical limitation of optical efficiency is ∼10% (note that the MoS_2 nanosieves still have efficiency below 10% if the contribution from the background is removed). Therefore, the fundamental method to enhance the efficiency of nanosieves further is to introduce phase modulation, which yields an efficiency limit of $\mathrm{sinc}^2(1/N)$ for an N-level phase[24]. If an additional metallic layer with high reflectance is employed below the meta-mirrors[25,26], the current reflective nanosieves will introduce a binary-phase modulation of reflected light from the meta-mirror and the substrate, thus leading to an efficiency limitation of ∼40%. Certainly, if the multi-level phase is employed, it will make the nanosieves behave like pure-phase metasurfaces[27].

5. Conclusions

In conclusion, we have proposed reflective photon nanosieves for holographic display. Much higher (by 3.5 times) efficiency than that of their counterpart transmission photon nanosieves is demonstrated experimentally. The hologram showed a broadband operation over 200 nm covering the visible range due to the subwavelength features of the meta-mirrors, with performance matching well with the simulation. Although the achieved efficiency in the reflective photon nanosieve is still lower than those of dielectric metasurfaces[28], it provides potential technology for optical display and anti-counterfeiting if the lower-cost nano-printing technique is employed for mass production.

Acknowledgement

This work was supported by the National Natural Science Foundation of China (Nos. 12134013 and 61875181), USTC Research Funds of the Double First-Class Initiative (No. YD2030002003), Fundamental Research Funds for the Central Universities in China, and CAS Poineer Hundred Talents Program. J. T. thanks the A*STAR IRG grant A2083c0058 and CRF grant. K. H. thanks the Centre for Micro and Nanoscale Research and Fabrication, University of Science and Technology of China for the support.

References

1. L. Kipp, M. Skibowski, R. L. Johnson, R. Berndt, R. Adelung, S. Harm, and R. Seemann, "Sharper images by focusing soft X-rays with photon sieves," Nature **414**, 184 (2001).
2. K. Huang, H. Liu, F. J. Garcia-Vidal, M. Hong, B. Luk'yanchuk, J. Teng, and C.-W. Qiu, "Ultrahigh-capacity non-periodic photon sieves operating in visible light," Nat. Commun. **6**, 7059 (2015).
3. Y. J. Liu, H. Liu, E. S. P. Leong, C. C. Chum, and J. H. Teng, "Fractal holey metal microlenses with significantly suppressed side lobes and high-order diffractions in focusing," Adv. Opt. Mater. **2**, 487 (2014).
4. S. Ishii, V. M. Shalaev, and A. V. Kildishev, "Holey-metal lenses: sieving single modes with proper phases," Nano Lett. **13**, 159 (2013).
5. Z. Xu, L. Huang, X. Li, C. Tang, Q. Wei, and Y. Wang, "Quantitatively correlated amplitude holography based on photon sieves," Adv. Opt. Mater. **8**, 1901169 (2020).
6. K. Huang, H. Liu, G. Si, Q. Wang, J. Lin, and J. Teng, "Photon-nanosieve for ultrabroadband and large-angle-of-view holograms," Laser Photonics Rev. **11**, 1700025 (2017).
7. J. Li, G. Si, H. Liu, J. Lin, J. Teng, and K. Huang, "Resonance-free ultraviolet metaoptics via photon nanosieves," Opt. Lett. **44**, 3418 (2019).
8. J. Park, K. Lee, and Y. Park, "Ultrathin wide-angle large-area digital 3D holographic display using a non-periodic photon sieve," Nat. Commun. **10**, 1304 (2019).
9. S. Mei, M. Q. Mehmood, S. Hussain, K. Huang, X. Ling, S. Y. Siew, H. Liu, J. Teng, A. Danner, and C.-W. Qiu, "Flat helical nanosieves," Adv. Fun. Mater. **26**, 5255 (2016).
10. M. Mehmood, S. Mei, S. Hussain, K. Huang, S. Siew, L. Zhang, T. Zhang, X. Ling, H. Liu, and J. Teng, "Visible-frequency metasurface for structuring and spatially multiplexing optical vortices," Adv. Mater. **28**, 2533 (2016).
11. X. Li, L. Chen, Y. Li, X. Zhang, M. Pu, Z. Zhao, X. Ma, Y. Wang, M. Hong, and X. Luo, "Multicolor 3D meta-holography by broadband plasmonic modulation," Sci. Adv. **2**, e1601102 (2016).
12. X. Ma, M. Pu, X. Li, C. Huang, Y. Wang, W. Pan, B. Zhao, J. Cui, C. Wang, and Z. Zhao, "A planar chiral meta-surface for optical vortex generation and focusing," Sci. Rep. **5**, 10365 (2015).
13. Y. Yang, G. Thirunavukkarasu, M. Babiker, and J. Yuan, "Orbital-angular-momentum mode selection by rotationally symmetric superposition of chiral states with application to electron vortex beams," Phys. Rev. Lett. **119**, 094802 (2017).
14. Z. Jin, D. Janoschka, J. Deng, L. Ge, P. Dreher, B. Frank, G. Hu, J. Ni, Y. Yang, and J. Li, "Phyllotaxis-inspired nanosieves with multiplexed orbital angular momentum," eLight **1**, 5 (2021).
15. L. Zhang, S. Mei, K. Huang, and C.-W. Qiu, "Advances in full control of electromagnetic waves with metasurfaces," Adv. Opt. Mater. **4**, 818 (2016).

16. D. Zhao, Z. Lin, W. Zhu, H. J. Lezec, T. Xu, A. Agrawal, C. Zhang, and K. Huang, "Recent advances in ultraviolet nanophotonics: from plasmonics and metamaterials to metasurfaces," Nanophotonics **10**, 2283 (2021).
17. A. Roberts, "Electromagnetic theory of diffraction by a circular aperture in a thick, perfectly conducting screen," J. Opt. Soc. Am. A **4**, 1970 (1987).
18. Z. Wang, G. Yuan, M. Yang, J. Chai, Q. Y. Steve Wu, T. Wang, M. Sebek, D. Wang, L. Wang, S. Wang, D. Chi, G. Adamo, C. Soci, H. Sun, K. Huang, and J. Teng, "Exciton-enabled meta-optics in two-dimensional transition metal dichalcogenides," Nano Lett. **20**, 7964 (2020).
19. D. Frese, B. Sain, H. Zhou, Y. Wang, L. Huang, and T. Zentgraf, "A wavelength and polarization selective photon sieve for holographic applications," Nanophotonics **10**, 4543 (2021).
20. M. Kalläne, J. Buck, S. Harm, R. Seemann, K. Rossnagel, and L. Kipp, "Focusing light with a reflection photon sieve," Opt. Lett. **36**, 2405 (2011).
21. K. Huang, F. Qin, H. Liu, H. Ye, C. W. Qiu, M. Hong, B. Luk'yanchuk, and J. Teng, "Planar diffractive lenses: fundamentals, functionalities, and applications," Adv. Mater. **30**, 1704556 (2018).
22. A. Taguchi, N. Hayazawa, K. Furusawa, H. Ishitobi, and S. Kawata, "Deep-UV tip-enhanced Raman scattering," J. Raman Spectrosc. **40**, 1324 (2009).
23. K. Huang, "Chirality and antiferromagnetism in optical metasurfaces," in *Chirality, Magnetism and Magnetoelectricity*, E. Kamenetskii, ed. (Springer Nature Switzerland AG, 2021).
24. D. A. Buralli, G. M. Morris, and J. R. Rogers, "Optical performance of holographic kinoforms," Appl. Opt. **28**, 976 (1989).
25. S. Sun, K.-Y. Yang, C.-M. Wang, T.-K. Juan, W. T. Chen, C. Y. Liao, Q. He, S. Xiao, W.-T. Kung, and G.-Y. Guo, "High-efficiency broadband anomalous reflection by gradient meta-surfaces," Nano Lett. **12**, 6223 (2012).
26. G. Zheng, H. Mühlenbernd, M. Kenney, G. Li, T. Zentgraf, and S. Zhang, "Metasurface holograms reaching 80% efficiency," Nat. Nanotechnol. **10**, 308 (2015).
27. K. Huang, Z. Dong, S. Mei, L. Zhang, Y. Liu, H. Liu, H. Zhu, J. Teng, B. Luk'yanchuk, J. K. Yang, and C. Qiu, "Silicon multi-meta-holograms for the broadband visible light," Laser Photonics Rev. **10**, 500 (2016).
28. K. Huang, J. Deng, H. S. Leong, S. L. K. Yap, R. B. Yang, J. Teng, and H. Liu, "Ultraviolet metasurfaces of ≈80% efficiency with antiferromagnetic resonances for optical vectorial anti-counterfeiting," Laser Photonics Rev. **13**, 1800289 (2019).